

Early strut protrusion and late neointima thickness in the Absorb bioresorbable scaffold: a serial wall shear stress analysis up to five years



Erhan Tenekecioglu¹, MD; Ryo Torii², PhD; Yuki Katagiri³, MD; Taku Asano³, MD; Rodrigo Modolo³, MD; Yosuke Miyazaki¹, MD, PhD; Ply Chichareon³, MD; Eric K.W. Poon⁴, PhD; Frank Gijssen⁵, PhD; Vikas Thondapu^{4,6}, MD; David van Klaveren⁷, PhD; Hans Jonker⁸, BSc; Andrew Ooi³, PhD; Peter Barlis⁴, MD, PhD; Carlos Collet³, MD; Yoshinobu Onuma¹, MD, PhD; Christos V. Bourantas^{9,10}, MD, PhD; Patrick W. Serruys^{1,11*}, MD, PhD

1. Department of Interventional Cardiology, Erasmus University Medical Center, Rotterdam, the Netherlands; 2. Department of Mechanical Engineering, University College London, London, United Kingdom; 3. Department of Cardiology, Academic Medical Center, Amsterdam, the Netherlands; 4. Department of Mechanical Engineering, Melbourne School of Engineering, University of Melbourne, Melbourne, Australia; 5. Department of Biomedical Engineering, Erasmus University Medical Center, Rotterdam, the Netherlands; 6. Melbourne Medical School, Faculty of Medicine, Dentistry & Health Sciences, University of Melbourne, Melbourne, Australia; 7. Department of Bioinformatics, Leiden University Medical Center, Leiden, the Netherlands; 8. Cardialysis, Rotterdam, the Netherlands; 9. Department of Cardiology, University College of London Hospitals, London, United Kingdom; 10. Department of Cardiology, Barts Heart Centre, London, United Kingdom; 11. Imperial College London, London, United Kingdom

E. Tenekecioglu and R. Torii contributed equally as co-first authors.

GUEST EDITOR: Adnan Kastrati, MD; Deutsches Herzzentrum, Munich, Germany

This paper also includes supplementary data published online at: <https://eurointervention.pconline.com/doi/10.4244/EIJ-D-18-00381>

KEYWORDS

- bioresorbable scaffolds
- drug-eluting stent
- optical coherence tomography
- other imaging modalities
- other technique

Abstract

Aims: The aim of the study was to evaluate the effect of strut protrusion (SP) on wall shear stress (WSS) and neointimal growth (NG) one and five years after implantation of an Absorb bioresorbable vascular scaffold.

Methods and results: Eight patients were selected from a first-in-man study. Following three-dimensional (3D) reconstruction of coronaries, WSS was quantified using Newtonian steady-flow simulation in each cross-section at 5° subunits (sectors) of the circumferential luminal surface. At one year, neointimal thickness (NT) was measured by optical coherence tomography (OCT) and correlated to WSS and SP post procedure. Median SP was 112.9 (90.8, 133.1) µm post implantation. Post procedure, a logarithmic inverse relationship between SP and post-implantation WSS ($r=-0.425$, $p<0.001$; correlation coefficients in a range from -0.143 to -0.553) was observed, whereas a correlation between baseline logarithm-transformed WSS (log-WSS) and NT ($r=-0.451$, $p<0.001$; correlation coefficients ranged from -0.140 to -0.662) was documented at one year. Mixed-effects analysis between baseline log-WSS and NT at follow-up yielded a slope of 30 µm/ln Pascal (Pa) and a y-intercept of 98 µm. As a result of NG, median flow area decreased from 6.91 (6.53, 7.48) mm² post implantation to 5.65 (5.47, 6.02) mm² at one-year follow-up ($p=0.01$) and to 5.75±1.37 mm² at five-year follow-up ($p=0.024$). However, the vessel surface exposed to low WSS (<1 Pa) decreased significantly post procedure (42%) to one year (35.9%) and five years (15.2%) (p -overall <0.0001).

Conclusions: SP disturbs laminar flow, creates regions of low WSS (<1.0 Pa) that are associated with NG and lumen area reduction. Low WSS post implantation reduced significantly at long-term follow-up. Thin struts with effective embedment would substantially reduce NG and accelerate homogenisation of WSS towards physiological values.

*Corresponding author: Imperial College London, London, SW7 2AZ, United Kingdom.

E-mail: patrick.w.j.c.serruys@gmail.com

Abbreviations

BRS	bioresorbable scaffolds
CFD	computational fluid dynamic
FA	flow area
NT	neointimal thickness
NTi	neointimal tissue
OCT	optical coherence tomography
QCA	quantitative coronary angiography
SP	strut protrusion
VW	vessel wall
WSS	wall shear stress

Introduction

Bioresorbable scaffolds (BRS) have ushered interventional cardiology into a new era of percutaneous treatment of coronary artery disease. BRS restores vasomotricity and vessel wall (VW) cyclic strain that are vital for VW metabolism¹. Local haemodynamics (LH), quantified as wall shear stress (WSS), have fundamental interaction with the VW². Scaffold coverage, strut thickness, protrusion and embedment have an influence on local WSS distribution^{3,4}. Following scaffold implantation, disruption of laminar flow triggers a cascade of reactions that may result in acute/subacute thrombosis, chronic exuberant neointimal tissue (NTi) and neoatherosclerosis⁵.

Optical coherence tomography (OCT)-based computational fluid dynamic (CFD) models provide assessment of LH at a detailed level not attainable even with experimental techniques⁶. In the present study, we investigated the effect of strut protrusion/embedment on post-implantation WSS (post-WSS) distribution and NTi formation at one-year and five-year follow-up.

Method

STUDY DESIGN

The details of the ABSORB cohort-B study (A Clinical Evaluation of the Everolimus-Eluting Bioresorbable Vascular Scaffold System in the Treatment of Patients with De-Novo Native Coronary Artery Lesions; NCT00856856) and treatment procedure have been previously described⁷. Eight cases with serial OCT were selected based on good image quality, minimal foreshortening and relative lack of curvature of the target vessel in two angiograms and clear visualisation of struts by OCT without major artefacts due to rotation, elongation and repetition of endoluminal structures due to cardiac motion⁸.

OCT IMAGE ACQUISITION

Intracoronary imaging was performed post procedure, at one year and five years in treated coronaries using a frequency-domain (FD) OCT system (C7-XR™ OCT; St. Jude Medical, St. Paul, MN, USA) with a pullback speed of 20 mm/sec. The details of image acquisition are shown in **Supplementary Appendix 1**.

OCT DATA ANALYSIS

OCT data were analysed off-line, using QCU-CMS software (Medis medical imaging systems, Leiden, the Netherlands)⁷.

The following data were acquired from OCT: endoluminal intra-scaffold flow area (FA), abluminal scaffold area, proximal and distal edge segment FA, percent (%) FA obstruction, neointima area and thickness⁷. The data acquired post implantation were used to investigate the relationship between post-implantation strut protrusion/embedment and post-WSS distribution. The data acquired at one-year follow-up were used to reconstruct two separate contours: firstly, the baseline luminal borders defined by splines connecting the adluminal sides of the struts (retrospective baseline model), and secondly the luminal contour at one-year follow-up (one-year follow-up model) delineating the inter-strut neointimal boundary as well as the covered struts (**Figure 1**).

EMBEDMENT/PROTRUSION ANALYSIS BY OCT

The strut embedment and protrusion were measured with a semi-automated method (QCU-CMS, version 4.69) (**Figure 2**)⁹.

CORONARY ARTERY RECONSTRUCTION

For the CFD study, three-dimensional (3D) reconstruction of the coronary artery was performed using a published methodology¹⁰. The details of 3D reconstruction are explained in **Supplementary Appendix 2**.

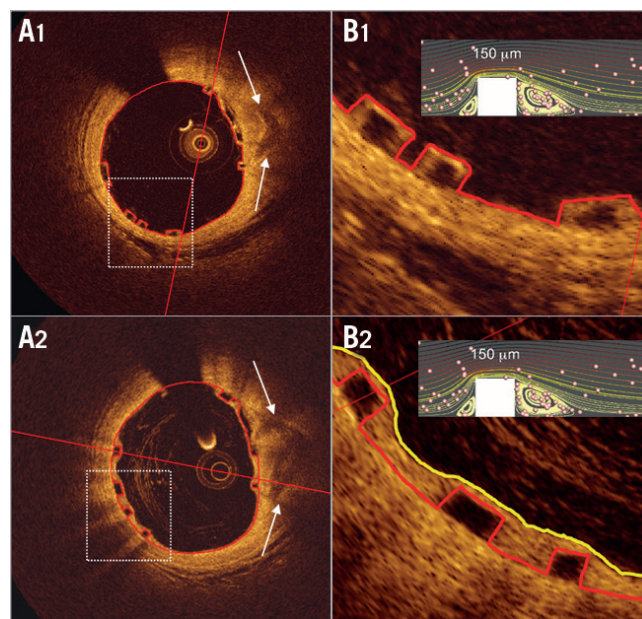


Figure 1. Neointimal tissue covers the polymeric struts at one year. In OCT the red contours superimposed on the lumen and strut boundaries in A1 and B1 are actual flow luminal contours post implantation, while in A2 and B2 the red contours still delineate the virtual and retrospective (one year later) flow luminal contours. For one-year retrospective analysis of virtual WSS post implantation, virtual post-procedure luminal borders in red were determined by the splines conjoining abluminal sides of the black core of the struts¹⁶. In B2, the yellow contour represents the actual flow luminal contour at one year once the struts have been covered by neointima. Inserted in B1 and B2 (right upper small panels) are CFD simulations that depict flow streamlines, cell tracking and flow reversals.

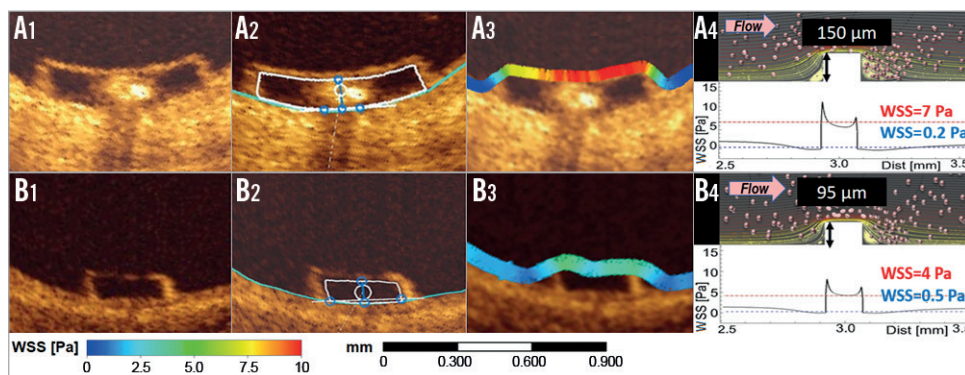


Figure 2. Strut thickness and strut protrusion post implantation determine the shear stress magnitudes on top of the strut and beside the struts. Panels A1 and B1 show two struts (Absorb and ArterioSorb™ [Arterius Ltd., Leeds, United Kingdom]) of different thickness (150 μm and 95 μm) and/or protrusion, with in A2 and B2 the interpolated luminal contour being located at the backside of the struts⁹. Panels A3 and B3 show colour-coded WSS overlying the strut, with high WSS in red on the top of the strut and low WSS in dark blue at the bottom of the strut. The thin strut (ArterioSorb) generates less of a WSS gradient between the top of the strut (indigo colour) and the bottom of the strut (light blue). CFD simulations shown in panels A4 and B4 depict streamlines, cell tracking indicating regions of flow reversal and WSS gradient (expressed in Pascals [Pa]) between the top (WSS value in red) and the bottom (WSS value in blue) of the strut⁴.

COMPUTATIONAL FLUID DYNAMIC STUDY

WSS was estimated by solving 3D Navier-Stokes equations (ANSYS CFX, Version 18.0; ANSYS, Inc., Canonsburg, PA, USA). WSS was measured in native and scaffolded segments in cross-sections along the axial direction per 200 μm interval and in circumferential per 5-degree subunits (sectors) in each cross-section, using an in-house algorithm (Figure 3). The details of the CFD study are explained in **Supplementary Appendix 3**.

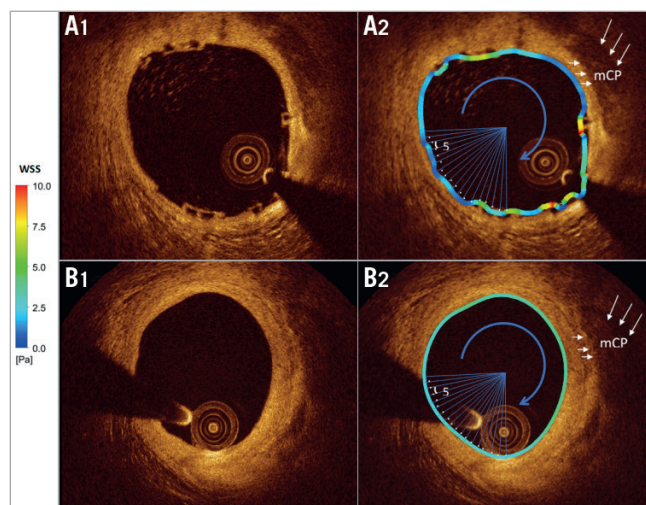


Figure 3. Homogenisation of the shear stress distribution at five-year follow-up. Post-WSS is quantified circumferentially in 5° subunits (sectors) (A1, A2) and at five years (B1, B2) over the luminal perimeter (see coloured barcode for WSS values). Each 5° subunit has one WSS value. Post implantation high WSS is usually observed on top of the strut and low WSS between the struts. At five years, WSS is homogeneously within physiological values (see barcode 2.5-5 Pa in green) (mCP: mixed calcified plaque).

STATISTICAL ANALYSIS

Data are expressed as mean \pm standard deviation or median and interquartile range. Pearson correlation coefficient and logarithmic regression analyses were implemented to investigate the association between baseline WSS, post-implantation protrusion and the neointimal thickness (NT) at follow-up. For WSS comparison between post implantation, one year and five years, a mixed-effects model was built on % increase of WSS from post implantation to one year and five years. All analyses were performed using statistical analysis programme SPSS, Version 23 (IBM Corp., Armonk, NY, USA), R V.3.2.3 and R package lme5 (R Foundation for Statistical Computing, Vienna, Austria)¹¹.

Results

PATIENT CHARACTERISTICS

In all cases (n=8), scaffolded segments were relatively straight and had a luminal centreline with <20 degree angulation¹². Five left anterior descending, two left circumflex and one right coronary artery were treated with an Absorb. All scaffolds had a diameter of 3.0 mm and a length of 18 mm. The expected scaffold diameter for the range of deployment pressures was 3.24 \pm 0.11 mm. Patient characteristics are shown in **Supplementary Table 1**. Procedural characteristics are shown in **Supplementary Table 2**. Pre-implantation, post-implantation, one-year and five-year quantitative coronary angiography (QCA) data are shown in **Table 1**.

OCT ANALYSIS RESULTS

OCT results are summarised in **Table 2**. The analyses were performed at device level (n=8). In-scaffold FA decreased from 6.91 (6.53, 7.48) mm² to 5.65 (5.47, 6.02) mm² at one year (p=0.01) and to 5.70 (5.10, 6.59) mm² at five years (p=0.024). At one year, neointimal proliferation (neointimal area: 1.4 [1.20, 2.01] mm², NT: 0.12 [0.06, 0.19] mm) was noticed in treated segments and

Table 1. Results of QCA analysis pre procedure, post procedure and at 5-year follow-up.

	Pre procedure (n:8) median (Q1, Q3)	Post procedure (n:8) median (Q1, Q3)	1-year follow-up (n:8) median (Q1, Q3)	5-year follow-up (n:8) median (Q1, Q3)	p-value (pre-post)	p-value (post-1 year)	p-value (1 year-5 year)	p-value (post-5 year)	p-value overall
In-scaffold lumen diameter, mm	2.21 (2.08, 2.30)	2.68 (2.54, 2.76)	2.42 (2.31, 2.54)	2.67 (2.31, 2.81)	0.001	0.021	0.998	0.212	0.03
In-scaffold minimum lumen diameter, mm	0.98 (0.88, 1.12)	2.33 (2.17, 2.41)	2.00 (1.91, 2.11)	2.23 (1.91, 2.34)	<0.0001	0.389	0.98	0.149	<0.0001
Interpolated reference vessel diameter, mm	2.54 (2.40, 2.55)	2.60 (2.53, 2.72)	2.45 (2.32, 2.51)	2.62 (2.34, 2.78)	0.353	0.047	0.986	0.997	0.228
In-scaffold percent diameter stenosis, %	63.2 (53.0, 65.8)	13.5 (9.9, 16.3)	16.0 (12.31, 17.8)	16.3 (12.5, 21.2)	<0.0001	0.985	0.99	0.86	<0.0001
In-scaffold acute absolute gain, mm	–	1.28 (0.98, 1.51)	–	–					
In-scaffold acute absolute recoil, mm	–	0.28 (0.14, 0.37)	–	–					
In-scaffold acute percent recoil, %	–	5.83 (–1.75, 9.25)	–	–					
In-scaffold absolute late lumen loss, mm	–	–	0.28 (0.14, 0.37)	0.04 (–0.04, 0.31)			0.476		0.476

Bonferroni adjustment was used for multiple comparisons. Post: post implantation; Pre: pre implantation; Q1: first quartile; Q3: third quartile

Table 2. OCT analysis post procedure, at one-year and five-year follow-up (in-scaffold and in-segment measurement).

	Post procedure (n _{scaffold} =8) median (Q1, Q3)	1-year follow-up (n _{scaffold} =8) median (Q1, Q3)	5-year follow-up (n _{scaffold} =8) median (Q1, Q3)	p-value (post-1 year)	p-value (1-year-5-year)	p-value (post-5 year)	p-value overall
Flow area, mm ²	6.91 (6.53, 7.48)	5.65 (5.47, 6.02)	5.70 (5.10, 6.59)	0.01	0.998	0.024	0.002
Abluminal scaffold area, mm ²	7.13 (6.86, 7.65)	7.11 (6.71, 7.67)		0.532			0.532
Strut area, mm ²	0.19 (0.17, 0.20)	0.17 (0.16, 0.18)		0.377		0.377	
Minimum flow area, mm ²	5.80 (5.28, 6.02)	4.16 (4.03, 4.60)	4.27 (3.20, 5.63)	0.021	0.98	0.091	0.010
Percentage flow area stenosis, %	4.47 (–6.71, 13.25)	17.1 (12.4, 24.3)	15.5 (11.7, 26.3)	0.50	0.998	0.466	0.22
Neointimal area, mm ²		1.4 (1.20, 2.01)					
Flow area in proximal edge segment, mm ²	6.69 (6.00, 9.91) ^o	6.22 (5.25, 8.40) [#]	5.63 (4.98, 6.32) ^o	0.322	0.998	0.951	0.344
Flow area in distal edge segment, mm ²	5.31 (4.56, 6.13) [‡]	5.16 (5.00, 5.74) [#]	5.68 (4.16, 6.65) ^Δ	0.99	0.88	0.99	0.72

^op-flow area between scaffolded segment and proximal edge segment post implantation=0.056; [#]p-flow area between scaffolded segment and distal edge segment post implantation <0.005; ^Δp-flow area between scaffolded segment and proximal edge segment at one year=0.39; [‡]p-flow area between scaffolded segment and distal edge segment at one year=0.47; ^op-flow area between scaffolded segment and proximal edge segment at five years=0.30; ^Δp-flow area between scaffolded segment and distal edge segment at five years=0.64; Post: post implantation; Pre: pre implantation; Q1: first quartile; Q3: third quartile; Bonferroni adjustment was used for multiple comparisons. In-scaffold post-procedure, n_{total cross-section}=705; In-scaffold five-year, n_{total cross-section}=686; Proximal edge segment post-procedure, n_{total cross-section}=572; Proximal edge segment 1-year, n_{total cross-section}=288; Proximal edge segment 5-year, n_{total cross-section}=512; Distal edge segment post-procedure, n_{total cross-section}=276; Distal edge segment 1-year, n_{total cross-section}=182; Distal edge segment 5-year, n_{total cross-section}=185

resulted in an increase of % FA stenosis from 4.47% (–6.71, 13.25) post implantation to 17.1% (12.4, 24.3) at one year and 15.5% (11.7, 26.3) at five years.

At five years, the regional differences in FA post implantation between non-scaffolded proximal/distal-edge and scaffolded segments disappeared (**Table 2**).

EMBEDMENT/PROTRUSION ANALYSIS RESULTS

The analyses were performed at cross-section and strut levels. All struts were well apposed to the VW. There were 5,038 struts analysed for embedment/protrusion in 556 OCT cross-sections.

At strut level, strut embedment was 54.2 (34.2, 77.4) μ m while the protrusion was 112.9 (90.9, 133.1) μ m. At cross-section level, strut embedment was 57.8 (45.5, 71.1) μ m while the protrusion was 109.3 (96.4, 121.6) μ m. Deployment/post-dilatation balloon pressures were found to have a slight effect on embedment depths ($r=0.14$, $p=0.049$).

WSS ANALYSIS POST IMPLANTATION AND AT FOLLOW-UP

Each CFD cross-section was divided into four quadrants and in each quadrant WSS was calculated at post-implantation baseline model, at retrospective baseline model, one-year model and

five-year model. Due to skewed WSS data, logarithmic transformation was implemented. Post-implantation median WSS was compared with the virtual WSS in the retrospective baseline model. The actual and virtual WSS peri-struts were compared at cross-section level ($n=630$) using a Bland-Altman approach and by linear regression analysis ($r=0.827$) (**Supplementary Figure 1A, Supplementary Figure 1B**). In mixed-effects analysis, WSS based on post-implantation CFD models (real post-implantation model) was comparable to WSS in retrospective baseline CFD models derived from one-year OCT data ($p=0.86$).

Post-implantation in-scaffold median WSS was 1.19 (0.84, 1.69) Pa, whereas median WSS in proximal and distal non-scaffolded edges was 1.82 (0.95, 3.10) Pa and 1.90 (1.03, 5.62) Pa, respectively (p -for difference between proximal non-scaffolded edge and scaffolded segment WSS=0.013, p -for difference in WSS between scaffolded and distal non-scaffolded edge<0.0001). **Figure 4** shows logarithmic inverse relationships between SP and post-WSS ($r=-0.425$, $p<0.001$; correlation coefficients ranged from -0.143 to -0.553).

At one year, in-scaffold median WSS was 1.26 (0.98, 1.60) Pa, whereas median WSS in the proximal non-scaffolded edge segment was 1.17 (0.67, 2.01) Pa and 1.81 (0.80, 3.44) Pa in the distal non-scaffolded edge segment. The median NT was 0.12 (0.06, 0.19) mm (area of neointima: 1.4 [1.20, 2.01] mm²). A statistically significant inverse correlation was noted between retrospective baseline log-WSS and NT at one year for all devices ($r=-0.451$, $p<0.005$; correlation coefficients ranged from -0.140 to -0.662) (**Figure 5**). Overall, mixed linear regression analysis between retrospective baseline log-WSS and NT at follow-up yielded a slope of 30 $\mu\text{m}/\ln(\text{Pa})$ and a y-intercept of 98 μm .

At five years, in-scaffold median WSS (1.92 [1.31, 2.81] Pa) was significantly higher than post procedure (1.19 [0.84, 1.69] Pa) ($p=0.0016$). Median WSS in proximal and distal non-scaffolded segments was not significantly different from scaffolded segment median WSS ($p=0.97$, $p=0.91$, respectively) (**Table 3**). The model fit with correlation structure was much better than the model fit without (likelihood ratio test $p<0.0001$) in comparisons between the time points.

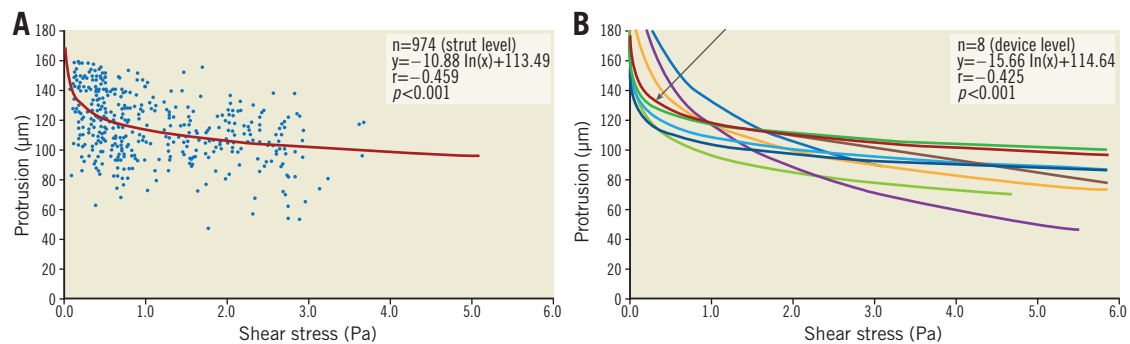


Figure 4. Inverse relationship between WSS and strut protrusion post implantation. A) Significant logarithmic inverse relationship between WSS (Pa) and SP (μm) at strut-level analysis for each cross-section of one device. B) The arrow identifies the single relationship exhibited in panel A among all the other logarithmic inverse relationships.

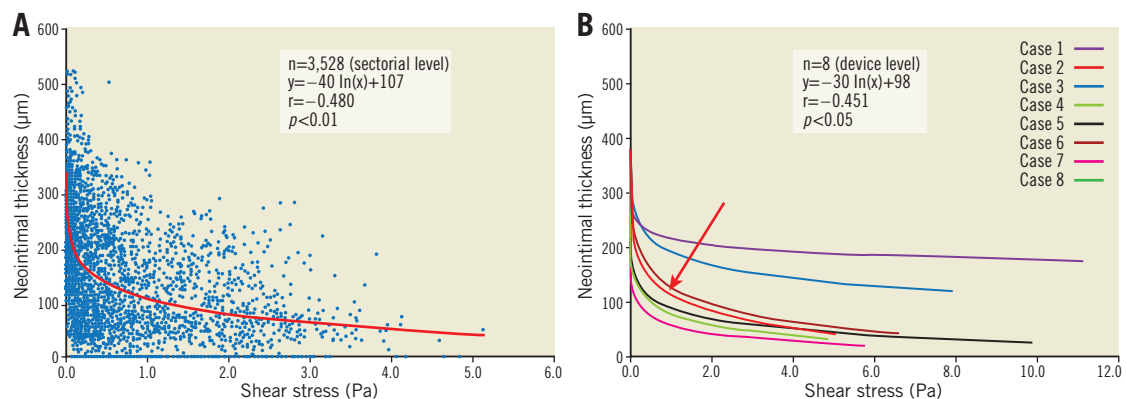


Figure 5. Inverse relationship between WSS post implantation and neointimal thickness at one-year follow up. A) Significant logarithmic inverse relationship between WSS and NT in one device displaying all the sectorial measurements obtained in that single device. B) The arrow identifies the neointima-WSS relationship for that specific device among all the other logarithmic inverse relationships observed in other devices.

Table 3. Results of WSS analysis (median values) post procedure, at one-year and at five-year follow-up.

	Post procedure (scaffolded segment, n=2,772) (proximal edge segment, n=2,248) (distal edge segment, n=1,108) median (Q1, Q3)	1-year follow-up (scaffolded segment, n=2,744) (proximal edge segment, n=1,920) (distal edge segment, n=528) median (Q1, Q3)	5-year follow-up (scaffolded segment, n=2,948) (proximal edge segment, n=2,124) (distal edge segment, n=700) median (Q1, Q3)	p-value (post-1 year)	p-value (1 year-5 year)	p-value (post-5-year)
WSS, proximal edge, Pa	^Δ 1.82 (0.95, 3.10)	[#] 1.17 (0.67, 2.01)	^Ω 1.63 (1.08, 2.42)	<0.0001	<0.0001	0.145
WSS, in-scaffold, Pa	1.19 (0.84, 1.69)	1.26 (0.98, 1.60)	1.92 (1.31, 2.81)	0.936	<0.00001	0.0016
WSS, distal edge, Pa	[‡] 1.90 (1.03, 5.62)	[¶] 1.81 (0.80, 3.44)	[∇] 1.82 (1.14, 3.10)	<0.0001	<0.0001	<0.0001
In-scaffold percent low ESS (<1 Pa), %	42.0%	35.9%	15.2%	<0.0001	<0.0001	<0.0001

^Δp<0.05, [‡]p<0.0001, [#]p<0.05, [¶]p<0.001, ^Ωp=0.11, [∇]p=0.89. n: total number of circumferential 4 quadrants per cross-section in the pullbacks performed serially in 8 scaffolds. p-values come from mixed-effects analysis. Post: post implantation; Pre: pre implantation; Q1: first quartile; Q3: third quartile

While post-WSS distribution was heterogeneous with numerous peri-strut zones of low WSS, at five years the distribution became more homogeneous (**Figure 6, Figure 7**). Vessel surface exposed to low WSS (<1 Pa) decreased significantly from 42.0% at baseline to 35.9% at one year and 15.2% at five years (p-overall <0.0001) (**Figure 8**).

Discussion

This is the first study to use serial OCT and CFD data to evaluate the effect of SP on WSS and NT at one-year and five-year follow-up. We have identified that: 1) the mean SP is 110±25 µm and only 36±15% of the strut thickness (157 µm) is embedded post implantation; 2) due to poor strut penetration, post-implantation

thick square-shaped struts induced flow disruptions with regions of very low WSS peri-strut; 3) the disrupted laminar WSS and areas of very low WSS with flow reversal at baseline determine the amount of peri-strut neointimal proliferation at one year; 4) at five years, due to neointimal coverage, WSS recovers homogeneous distribution with physiological values; 5) at the edges of the scaffolded region, initial post-procedural step-up and step-down in WSS disappeared at five years.

THE IMPACT OF SP ON POST-WSS AND NEOINTIMAL REGENERATION AT ONE YEAR

Due to the wide footprint of the Absorb, strut embedment is not easily achievable. The square shape and initial contact radius of

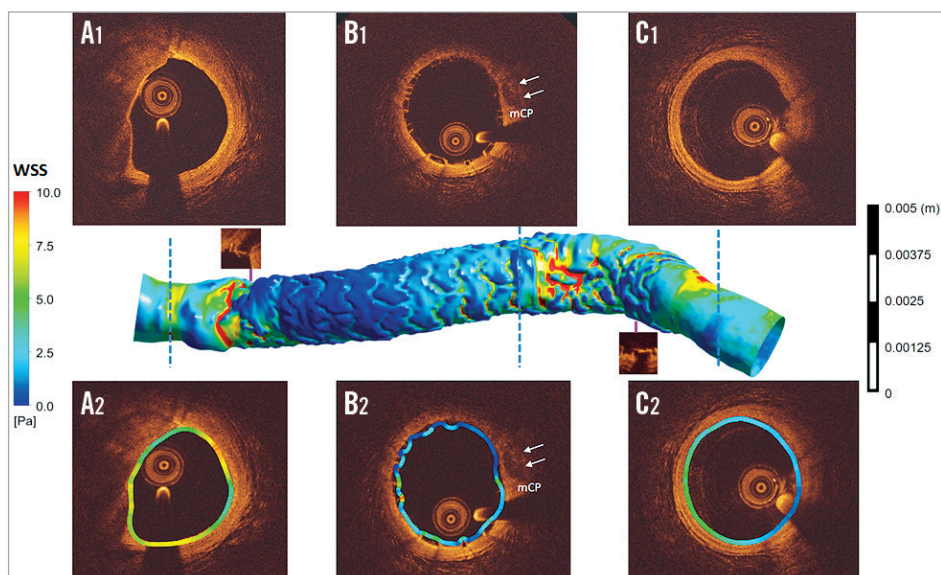


Figure 6. Post-implantation shear stress distribution in scaffold-implanted vessel. WSS was analysed post implantation in the proximal non-scaffolded segment (A1, A2), in scaffolded segments (B1, B2) and in the distal non-scaffolded edge segment (C1, C2). In the scaffolded segment, due to larger luminal area and strut protrusion, WSS in the inter-strut luminal surface shows a peri-strut area of very low WSS (dark blue in B2). At the inlet and outlet of the scaffold, the non-scaffolded segment shows a short region of high WSS in red (mCP: mixed calcified plaque).

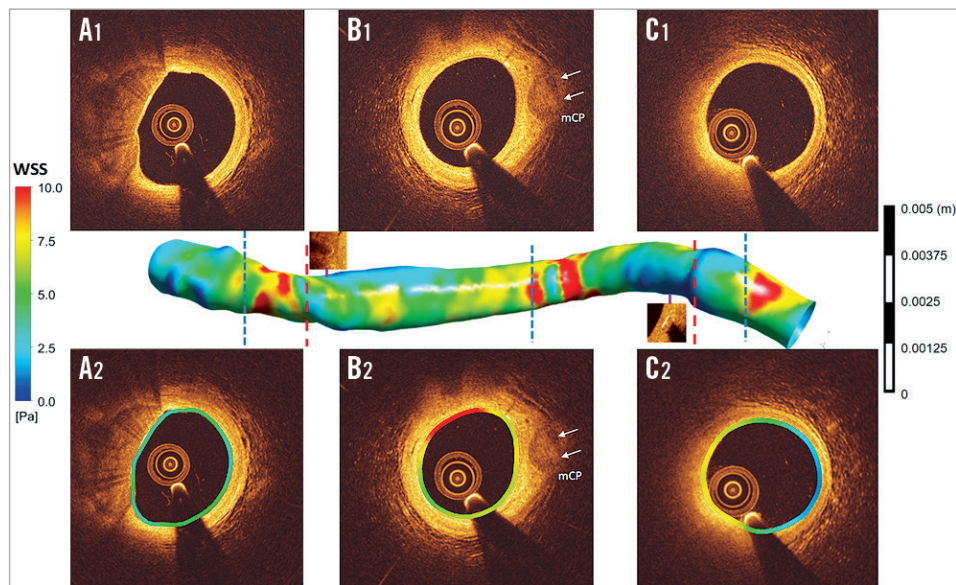


Figure 7. Shear stress distribution in scaffold-implanted vessel at five-year follow up. At five years, WSS was analysed in the proximal non-scaffolded edge (A1, A2), in scaffolded segments (B1, B2) and in the distal non-scaffolded edge (C1, C2). Compared to the corresponding cross-sections in the post-implantation CFD model in Figure 5, WSS distribution becomes more homogeneous and has more physiological values (colour-coded green and yellow) ranging between 5 and 7.5 Pa in the scaffolded segment identified on OCT by the radiopaque markers. The inlet and outlet of the scaffold still show an area of high WSS in red. At follow-up, the lumen became smooth without significant topographic obstacles which could disrupt the flow (mCP: mixed calcified plaque).

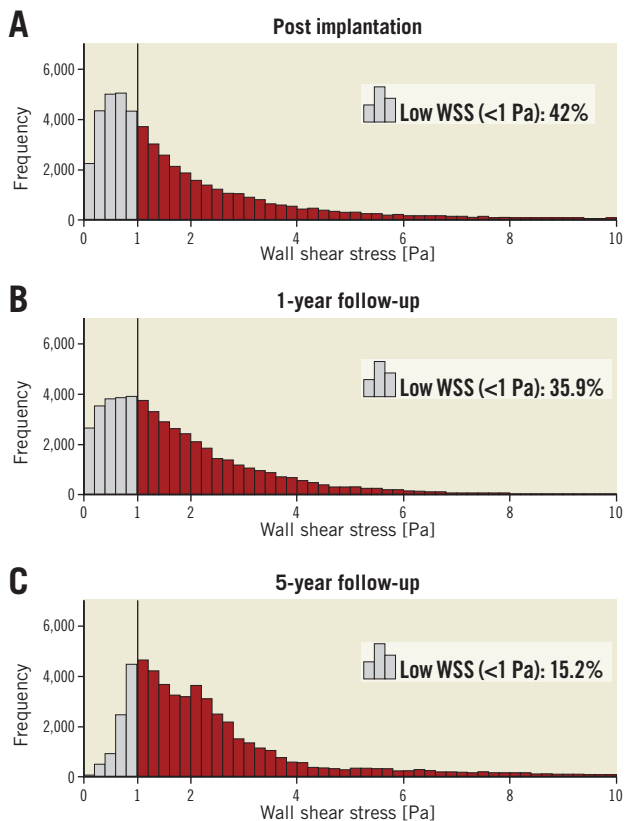


Figure 8. Histograms of WSS post implantation, at one year and at five years. The percentage of low WSS (<1 Pa) was 42% post implantation (A), 35.9% at one year (B) and 15.2% at five years (C).

the struts impede penetration according to the principles of contact mechanics¹³. The penetration of the strut is directly related to the strut width which is based on Pascal's law of pressure (Pressure=Force/Area). As the strut width increases, the pressure required for wall penetration will increase which may reduce the strut embedment considerably. With poor penetration, thick struts stand as obstacles, creating flow separations, eddies and stasis around the struts, resulting in low WSS peri-strut. On the other hand, the strut surface induces higher WSS, creating a gradient in WSS between the top and bottom of the struts¹⁴. The disturbed flow and oscillatory WSS promote biological changes producing a well-established environment for thrombus formation and neointimal hyperplasia (NH) through activation of athero-promoting genes¹⁵. The NTi on the strut surface is much less accentuated than in the inter-strut zones¹⁶. Over time, this mechanobiological modulation of tissue proliferation dissipates the WSS micro-gradient as the proliferating tissue between the struts fills inter-strut zones. NTi continues to develop until it reaches the strut surface and the thicker the struts are, the thicker the neointima will be.

With thinner struts and deeper VW embedment, protrusion is reduced and recirculation and stagnation around the struts will be smaller⁵. In case of thinner struts with good penetration, neointimal growth (NG) will inevitably be limited with less lumen area reduction¹⁷.

IMPROVEMENT IN WSS AT LONG-TERM FOLLOW-UP

Following scaffold implantation, barotrauma stretch-induced arterial injury changes the smooth muscle cell (SMC) phenotype from

contractile to synthetic and triggers SMC migration towards the subintima where they secrete abundant proteoglycans forming the bulk of the stenotic mass¹⁸. Mechanical stretch also engenders inflammatory reactions in the intima and adventitia. The antiproliferative drug eluted from the scaffold aims to eliminate the early inflammatory reaction secondary to the barotrauma. However, 80% of the antiproliferative drug is eluted from the scaffold by 30 days⁷. The limited duration of antiproliferative agent release has no significant effect on long-term NG that is influenced by other factors such as LH. Apparently, increased and sustained laminar WSS at follow-up is an inhibiting factor for further cellular proliferation¹⁹.

Step-up and step-down in luminal dimensions at the inlet and outlet of the scaffold generate macro-changes in WSS and modulate neointimal proliferation that will ultimately homogenise luminal dimensions in the proximal, distal and scaffolded segments²⁰. The morphological improvement in transitional zones was completed at one year²¹.

METHODOLOGICAL CHALLENGES IN ASSESSING WSS AND NEOINTIMA

During implantation, the thick struts of the Absorb are barely embedded and highly protruding. These protruding struts disturb laminar flow around the struts. At that stage, the best approach to describe flow patterns is proposed by Gogas et al, depicting five sites of WSS assessment: proximal inter-strut, proximal peri-strut, on top of the strut, distal peri-strut and inter-strut space distal to the strut²².

At one year, translucency and volume of the strut remain essentially unchanged. By interpolating lumen contour from the embedded struts, it is possible to reconstruct the lumen contour (for a retrospective post-implantation model). It has been appealing to compute retrospectively peri-strut WSS (virtual baseline WSS) and correlate the current neointima at one year, as this approach enables perfect co-localisation and matched assessment of the post-WSS with current NG at one year (**Figure 2**)¹⁶.

At five years, the struts and initial lumen contour are undetectable, and the luminal surface is smooth and homogeneous. The only feasible method of surface analysis was to subdivide the luminal perimeter into subunits of 5° sectors. To standardise the analysis method and render the WSS analysis comparable for three periods of acquisition, post implantation, one year and five years, we applied a subunit sector approach to those three periods¹⁶.

Limitations

The main limitation of the present study is that, to investigate the relationship between post-WSS and NT at one year, a retrospective 3D vessel model was implemented using one-year OCT data. This was done to overcome potential discrepancies in corresponding OCT frames, regarding the circumferential strut distribution between post-implantation and one-year OCT and to associate post-WSS and follow-up neointima as accurately as possible. The second limitation is the small number

of observations. Several criteria were implemented for filtering suitable cases to investigate the effect of SP on post-WSS and NH at one year. 1) To prevent any effect of swirling flow due to vessel curvature, on the scaffolded segment WSS distribution, we did not include the cases with curvature. 2) The cases without two angiographic projections with at least a >25 degree difference could not be reconstructed. 3) To investigate the alteration in WSS at one year and five years, the cases with truly serial OCT imaging post implantation, at one year and at five years were recruited.

Conclusions

Following Absorb implantation, the local flow micro-environment around the protruding struts is characterised by alternance of high and low WSS. SP and disrupted local WSS appear to be important determinants of NG. The thickness of the struts and intensity of the flow disturbance predetermine the thickness of the inter-strut neointima. With time, newly constituted intimal lining improved the luminal surface with homogenisation of the WSS towards physiological values at long-term follow-up. Despite the initial bulky structure of the quadratic struts, the VW recovered its smooth surface to re-establish a *de novo* laminar WSS profile, following biointegration of the scaffold into the VW.

Guest Editor

This paper was guest edited by Adnan Kastrati, MD; Deutsches Herzzentrum, Munich, Germany.

Impact on daily practice

The fundamental issue of the polymeric struts in PLLA is their lack of tensile strength and radial force that have to be compensated for by their thickness and large footprint, pre-empting VW embedment and their quick coverage by neointima. Thereby, SP and its disturbing impact on laminar flow and WSS predetermine the thickness of the neointima. Although the present observation is hypothesis-generating, recent preclinical and clinical observations with thinner and circular struts have demonstrated a causative relationship between embedment (more) and WSS disturbance (less)⁴. Long-term follow-up will confirm or disprove a causative relationship between strut thickness and the thickness of the neointima with new-generation bioresorbable scaffolds with thinner and circular struts.

Funding

E. Tenekecioglu has received a research grant from the Scientific and Technological Council of Turkey (TUBITAK).

Conflict of interest statement

P.W. Serruys and Y. Onuma are members of the International Advisory Board of Abbott Vascular. The other authors have no conflicts of interest to declare. The Guest Editor has no conflicts of interest to declare.

References

1. Serruys PW, Garcia-Garcia HM, Onuma Y. From metallic cages to transient bioresorbable scaffolds: change in paradigm of coronary revascularization in the upcoming decade? *Eur Heart J*. 2012;33:16-25b.
2. Slager CJ, Wentzel JJ, Gijssen FJ, Schuurbijs JC, van der Wal AC, van der Steen AF, Serruys PW. The role of shear stress in the generation of rupture-prone vulnerable plaques. *Nat Clin Pract Cardiovasc Med*. 2005;2:401-7.
3. Tenekecioglu E, Torii R, Bourantas C, Crake T, Zeng Y, Sotomi Y, Onuma Y, Yilmaz M, Santoso T, Serruys PW. Preclinical assessment of the endothelial shear stress in porcine-based models following implantation of two different bioresorbable scaffolds: effect of scaffold design on the local haemodynamic micro-environment. *EuroIntervention*. 2016;12:1296.
4. Tenekecioglu E, Torii R, Bourantas CV, Al-Lamee R, Serruys PW. Non-Newtonian pulsatile shear stress assessment: a method to differentiate bioresorbable scaffold platforms. *Eur Heart J*. 2017;38:2570.
5. Jimenez JM, Davies PF. Hemodynamically driven stent strut design. *Ann Biomed Eng*. 2009;37:1483-94.
6. Murphy J, Boyle F. Predicting neointimal hyperplasia in stented arteries using time-dependant computational fluid dynamics: a review. *Comput Biol Med*. 2010;40:408-18.
7. Serruys PW, Onuma Y, Ormiston JA, de Bruyne B, Regar E, Dudek D, Thuesen L, Smits PC, Chevalier B, McClean D, Koolen J, Windecker S, Whitbourn R, Meredith I, Dorange C, Veldhof S, Miquel-Hebert K, Rapoza R, Garcia-Garcia HM. Evaluation of the second generation of a bioresorbable everolimus drug-eluting vascular scaffold for treatment of de novo coronary artery stenosis: six-month clinical and imaging outcomes. *Circulation*. 2010;122:2301-12.
8. Okamura T, Onuma Y, Garcia-Garcia HM, Bruining N, Serruys PW. High-speed intracoronary optical frequency domain imaging: implications for three-dimensional reconstruction and quantitative analysis. *EuroIntervention*. 2012;7:1216-26.
9. Sotomi Y, Tateishi H, Suwannasom P, Dijkstra J, Eggermont J, Liu S, Tenekecioglu E, Zheng Y, Abdelghani M, Cavalcante R, de Winter RJ, Wykrzykowska JJ, Onuma Y, Serruys PW, Kimura T. Quantitative assessment of the stent/scaffold strut embedment analysis by optical coherence tomography. *Int J Cardiovasc Imaging*. 2016;32:871-83.
10. Bourantas CV, Papafaklis MI, Lakkas L, Sakellarios A, Onuma Y, Zhang YJ, Muramatsu T, Diletti R, Bizopoulos P, Kalatzis F, Naka KK, Fotiadis DI, Wang J, Garcia Garcia HM, Kimura T, Michalis LK, Serruys PW. Fusion of optical coherence tomographic and angiographic data for more accurate evaluation of the endothelial shear stress patterns and neointimal distribution after bioresorbable scaffold implantation: comparison with intravascular ultrasound-derived reconstructions. *Int J Cardiovasc Imaging*. 2014;30:485-94.
11. Bates D, Mächler M, Bolker B, Walker S. Fitting Linear Mixed-Effects Models Using lme4. *Journal of Statistical Software*. 2015;67:1-48.
12. Gomez-Lara J, Garcia-Garcia HM, Onuma Y, Garg S, Regar E, De Bruyne B, Windecker S, McClean D, Thuesen L, Dudek D, Koolen J, Whitbourn R, Smits PC, Chevalier B, Dorange C, Veldhof S, Morel MA, de Vries T, Ormiston JA, Serruys PW. A comparison of the conformability of everolimus-eluting bioresorbable vascular scaffolds to metal platform coronary stents. *JACC Cardiovasc Interv*. 2010;3:1190-8.
13. Johnson KL. Contact Mechanics. Cambridge, UK: Cambridge University Press; 1987.
14. LaDisa JF Jr, Olson LE, Molthen RC, Hettrick DA, Pratt PF, Hardel MD, Kersten JR, Warltier DC, Pagel PS. Alterations in wall shear stress predict sites of neointimal hyperplasia after stent implantation in rabbit iliac arteries. *Am J Physiol Heart Circ Physiol*. 2005;288:H2465-75.
15. Chien S. Mechanotransduction and endothelial cell homeostasis: the wisdom of the cell. *Am J Physiol Heart Circ Physiol*. 2007;292:H1209-24.
16. Bourantas CV, Papafaklis MI, Kotsia A, Farooq V, Muramatsu T, Gomez-Lara J, Zhang YJ, Iqbal J, Kalatzis FG, Naka KK, Fotiadis DI, Dorange C, Wang J, Rapoza R, Garcia-Garcia HM, Onuma Y, Michalis LK, Serruys PW. Effect of the endothelial shear stress patterns on neointimal proliferation following drug-eluting bioresorbable vascular scaffold implantation: an optical coherence tomography study. *JACC Cardiovasc Interv*. 2014;7:315-24.
17. Kastrati A, Mehilli J, Dirschinger J, Dotzer F, Schühlen H, Neumann FJ, Fleckenstein M, Pfafferott C, Seyfarth M, Schömig A. Intracoronary stenting and angiographic results: strut thickness effect on restenosis outcome (ISAR-STEREO) trial. *Circulation*. 2001;103:2816-21.
18. Russo RJ, Silva PD, Yeager M. Coronary artery overexpansion increases neointimal hyperplasia after stent placement in a porcine model. *Heart*. 2007;93:1609-15.
19. Carlier SG, van Damme LC, Blommerde CP, Wentzel JJ, van Langenhove G, Verheye S, Kockx MM, Knaapen MW, Cheng C, Gijssen F, Duncker DJ, Stergiopoulos N, Slager CJ, Serruys PW, Krams R. Augmentation of wall shear stress inhibits neointimal hyperplasia after stent implantation: inhibition through reduction of inflammation? *Circulation*. 2003;107:2741-6.
20. Tateishi H, Suwannasom P, Sotomi Y, Nakatani S, Ishibashi Y, Tenekecioglu E, Abdelghani M, Cavalcante R, Zeng Y, Grundeken MJ, Albuquerque FN, Veldhof S, Onuma Y, Serruys PW; investigators of the ABSORB Cohort B study. Edge Vascular Response After Resorption of the Everolimus-Eluting Bioresorbable Vascular Scaffold - A 5-Year Serial Optical Coherence Tomography Study. *Circ J*. 2016;80:1131-41.
21. Torii R, Tenekecioglu E, Bourantas C, Poon E, Thondapu V, Gijssen F, Sotomi Y, Onuma Y, Barlis P, Ooi ASH, Serruys PW. Five-year follow-up of underexpanded and overexpanded bioresorbable scaffolds: self-correction and impact on shear stress. *EuroIntervention*. 2017;12:2158-9.
22. Gogas BD, Yang B, Piccinelli M, Giddens DP, King SB 3rd, Kereiakes DJ, Ellis SG, Stone GW, Veneziani A, Samady H.

Novel 3-Dimensional Vessel and Scaffold Reconstruction Methodology for the Assessment of Strut-Level Wall Shear Stress After Deployment of Bioresorbable Vascular Scaffolds From the ABSORB III Imaging Substudy. *JACC Cardiovasc Interv.* 2016;9:501-3.

Supplementary data

Supplementary Appendix 1. OCT image acquisition and OCT data analysis.

Supplementary Appendix 2. Coronary artery reconstruction.

Supplementary Appendix 3. Computational fluid dynamic study.

Supplementary Figure 1. Agreement and correlation between the retrospective post-implantation and real post-implantation models.

Supplementary Table 1. Baseline characteristics of the studied population (N=8, lesions=8).

Supplementary Table 2. Procedural characteristics.

*The supplementary data are published online at:
[https://eurointervention.pcronline.com/
doi/10.4244/EIJ-D-18-00381](https://eurointervention.pcronline.com/doi/10.4244/EIJ-D-18-00381)*



Supplementary data

Supplementary Appendix 1. OCT image acquisition and OCT data analysis

A non-occlusive flushing technique involved injection of angiographic contrast medium for blood clearance. The flow area (FA) of the scaffolded segment and 5 mm segments adjacent to the proximal and distal scaffold edges were analysed at 200 μm intervals by an independent core laboratory (Cardialysis, Rotterdam, the Netherlands). The data acquired post implantation were used to investigate the relationship between post-implantation strut protrusion/embedment and post-implantation WSS distribution. The data acquired at 1-year follow-up were used to reconstruct two separate contours: firstly, the baseline luminal borders defined by splines connecting the adluminal sides of the struts (retrospective baseline model), and secondly the luminal contour at 1-year follow-up (one-year follow-up model) delineating the inter-strut neointimal boundary as well as the covered struts (**Figure 1**). The rationale for this approach was to optimise the topographical relationship between WSS evaluation and neointimal growth at one-year follow-up and avoid complex and inaccurate co-localisation and matching on OCT cross-sections of struts visualised post procedure and at 1 year. After full complete bioresorption, the five-year luminal contours on OCT were used to assess the WSS at five years.

Supplementary Appendix 2. Coronary artery reconstruction

The radiopaque markers and the anatomical landmarks (i.e., the side branches), identified both on angiography and on OCT, were used to define the scaffolded segment and the 5 mm proximal-distal native vessel segments. In the region of interest (ROI), the scaffolded and the proximal-distal non-scaffolded vessel segments were analysed at 200 μm intervals. Post implantation, the FA was delineated in the non-scaffolded segments by the luminal border and in the scaffolded segments by

the endoluminal side of the struts and by the luminal surface borders between the struts. At one-year follow-up, for the retrospective analysis of the WSS post implantation, post-procedure luminal borders were determined by the splines conjoining the abluminal sides of the struts. The luminal surfaces at one-year (one-year follow-up model) and five-year (five-year follow-up model) follow-up were established by the endoluminal borders of the grown neointima.

Two end-diastolic angiographic projections with $>30^\circ$ angle difference were selected which portrayed the most distal and proximal anatomical landmark detected also in the FD-OCT images [7]. In order to delineate the lumen contours and to estimate the centreline of the lumen, the two centrelines from the angiograms were used to form the 3D luminal centreline. In this reconstruction, the 3D luminal centreline derived from the angiographic projections was used as a “backbone”. The centre of mass (i.e., centroid) of the lumen area in FD-OCT images was established and lumen borders obtained from FD-OCT were placed perpendicularly onto the 3D lumen centreline in equidistant locations, positioning the lumen centroids on the 3D centreline. The orientation of side branches was used for the absolute rotational orientation of the FD-OCT cross-sections. The lumen 3D boundary points were combined to obtain the FD-OCT-based lumen geometry in 3D.

Supplementary Appendix 3. Computational fluid dynamic study

To determine the impact of scaffold design on the local haemodynamic microenvironment, the mesh density around the struts and in the near wall flow boundary zone was elaborated to have an average element edge of 20 μm (less than 1/7 of the strut thickness). Blood was treated as a homogeneous, Newtonian fluid with a viscosity of 0.0035 Pa.s and a density of 1,050 kg/m^3 . A steady and parabolic flow velocity profile was imposed at the inlet of the 3D models. Blood flow for each reconstruction was estimated by measuring, in the two angiographic projections, the

number of frames required for the contrast agent to pass from the inlet to the outlet of the reconstructed segment, the volume of the reconstructed segment and the cine frame rate [9]. The arterial wall was considered to be rigid. No-slip conditions were imposed at the scaffold surface and vessel luminal surface. At the outlet of the model zero-pressure conditions were imposed. WSS at the luminal surface and strut surface was calculated as the product of blood viscosity and the gradient of blood velocity at the wall and strut surface.

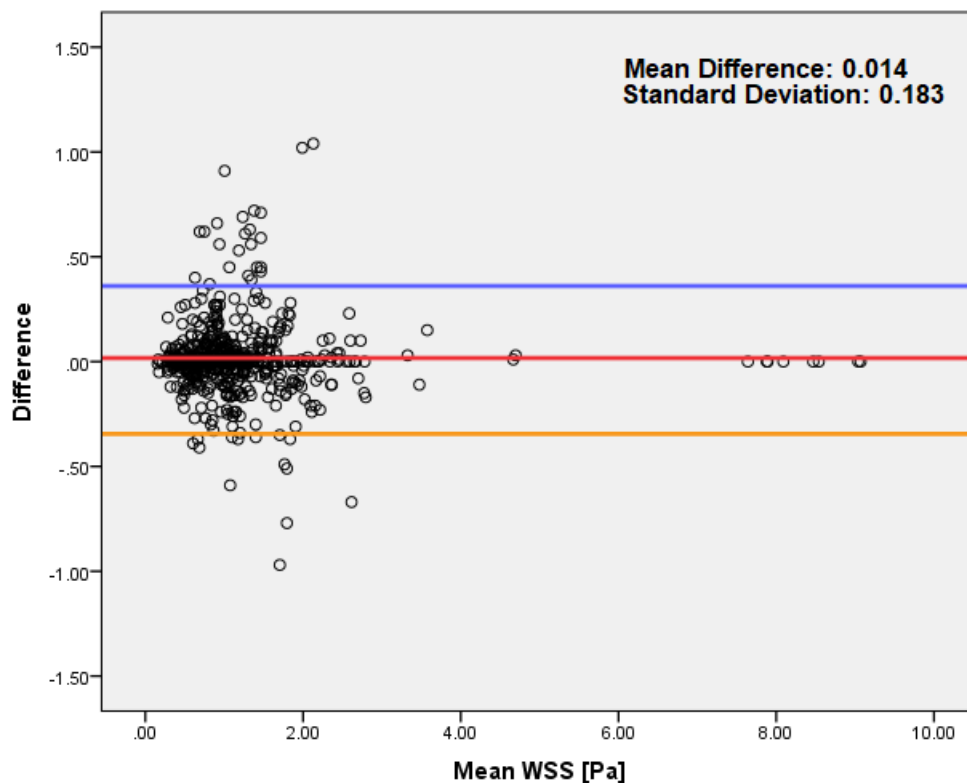
Statistical analysis

Normality of distribution was tested using the Kolmogorov-Smirnov test. Paired variables were compared using a general linear model with Bonferroni adjustment between multiple timepoints. Categorical variables were compared using Pearson's chi-square test or Fisher's exact test, as appropriate. For WSS comparison between post implantation, 1-year and 5-year follow-up, a mixed-effects model was built on % increase of WSS from post implantation to 1-year and 5-year follow-up. The model was set with fixed effects on log-WSS with standard deviations and intercept, and random-effects on patient ID. Since WSS values in adjacent cross-sections are related to each other and are not independent from each other, there are unavoidable correlations between the WSS values in sequential cross-sections. Therefore, a special correlation structure was implemented based on Euclidian distances between the locations where 5-degree sectorial WSS was quantified. The correlation structure was incorporated into the mixed-effects model within random effects.

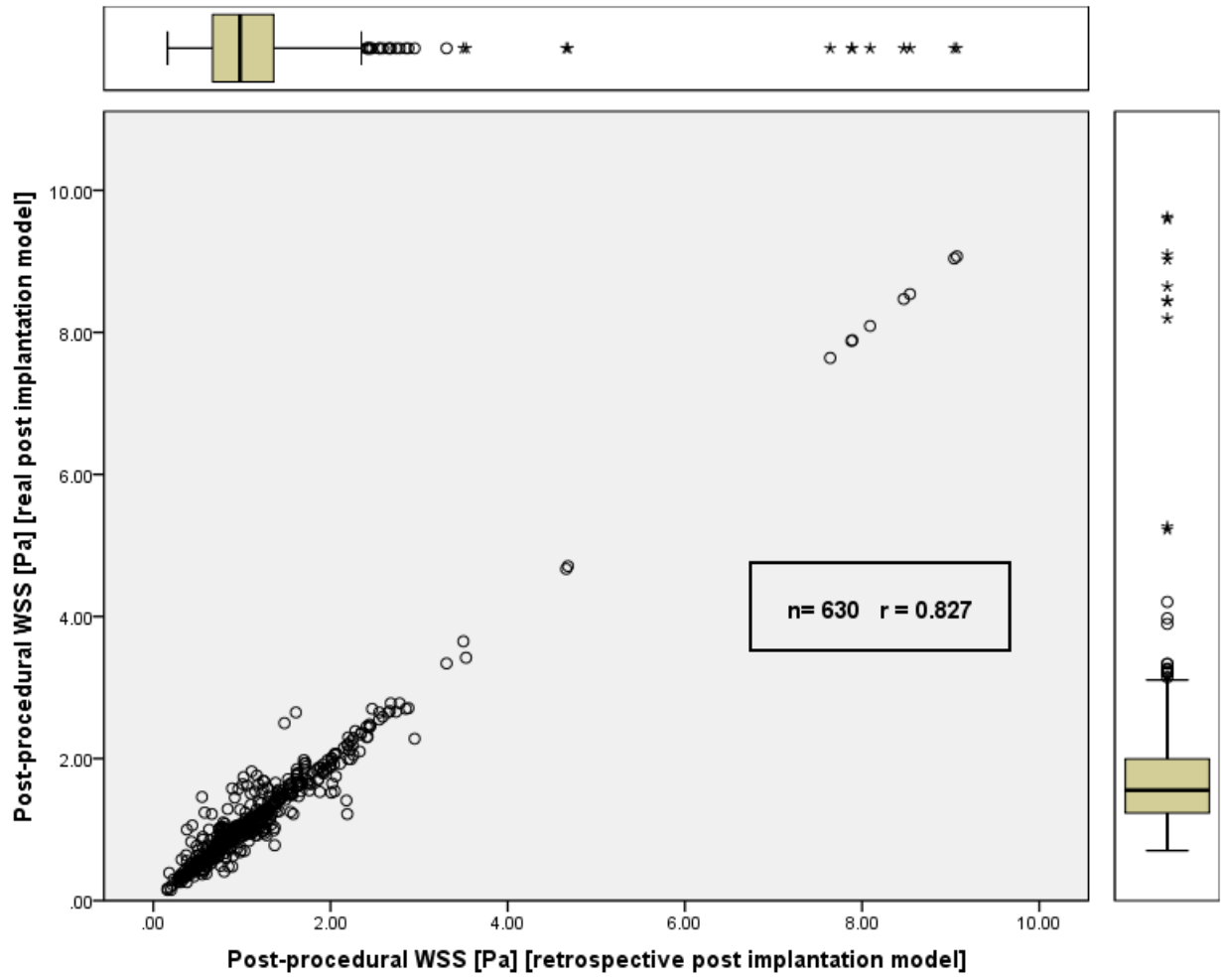
Supplementary Figure 1. Agreement and correlation between the retrospective post-implantation and real post-implantation models.

- A.** Bland-Altman plots showing a narrow level of agreement (LOA) in the cross-section level (n=630) of median WSS values between the retrospective post-implantation and real post-implantation models. The mean difference was 0.014 and LOAs for WSS were 0.38 and -0.17.
- B.** Linear regression graph showing a high correlation coefficient ($r=0.827$) between cross-section level median WSS (n=630) from the retrospective post-implantation model and the real post-implantation model.

A.



B.



Supplementary Table 1. Baseline characteristics of the studied population (N=8, lesions=8).

Age, yrs	62±8
Male	5 (63)
Hypertension	5 (63)
Hypercholesterolaemia	6 (75)
Diabetes mellitus	0 (0)
Current smoking	3 (38)
Prior percutaneous coronary intervention	1 (12)
Prior myocardial infarction	2 (25)
Stable angina	7 (88)
Unstable angina	1 (12)
Silent ischaemia	0 (0)
Treated vessel	
Left anterior descending artery	5 (63)
Left circumflex artery	2 (25)
Right coronary artery	1 (12)
Ramus intermedius	0 (0)

Values are mean±SD or n (%).

Supplementary Table 2. Procedural characteristics.

		N=8, L=8
ACC/AHA lesion class	A	0% (0)
	B1	63% (5)
	B2	38% (3)
	C	0% (0)
Predilatation		100% (8/8)
Predilatation pressure, atm		11.00±2.20
Diameter of scaffolds, mm		3.00±0.0
Expected scaffold diameter, mm		3.24±0.11
Total length of study devices, mm		18.0±0.0
Nominal scaffold area, mm ²		8.26±0.56
Deployment pressure, atm		11.50±2.56
Post-dilatation		63% (5)
Post-dilatation pressure, atm		16.0±3.27
Procedure complication		0 (0)
Clinical device success		100% (8/8)
Clinical procedure success		100% (8/8)

Values are mean±SD or n (%).